# Analytical approach to Coulomb focusing in strong-field ionization. II. Multiple recollisions

Jiří Daněk,* Karen Z. Hatsagortsyan,† and Christoph H. Keitel
*Max-Planck-Institut für Kernphysik, Saupfercheckweg 1, 69117 Heidelberg, Germany*

(Received 27 March 2018; revised manuscript received 29 April 2018; published 13 June 2018)

An analytical method for treating Coulomb focusing in strong-field ionization in a linearly polarized laser field has been proposed in the first paper of this series, where analytical formulas have been derived for the Coulomb momentum transfer to the tunneled electron at the tunnel exit and due to rescatterings. In this paper, we analytically investigate a buildup of the Coulomb momentum transfer during multiple laser driven recollisions of the tunneled electron on the parent ion. We find that the momentum transfer at rescattering events, while being a perturbation with respect to the instantaneous electron momentum at the rescattering, induces a significant nonperturbative contribution to the total momentum transfer. Moreover, we show that the higher-order recollisions contribute considerably to the total momentum transfer and cannot be omitted for the proper description of the Coulomb focusing. We also show that our analytical approach to Coulomb focusing is well suitable for proper description of the Coulomb focusing cusps of the photoelectron momentum distribution at energies larger than 50 meV.

DOI: 10.1103/PhysRevA.97.063410

## I. INTRODUCTION

Rescattering is one of the key concepts in strong-field physics [1]. While hard rescatterings with a small impact parameter are the reason for above-threshold ionization [2], high-order-harmonic generation [3], and nonsequential double ionization [4], soft rescatterings with a large impact parameter induce Coulomb focusing, that is, squeezing the photoelectron momentum space transverse to the laser polarization direction [5–7]. The recollision physics is more pronounced in mid-IR laser fields [8], because the photoelectron dynamics is more quasiclassical in this case, which allowed the recent discovery of new Coulomb effects, such as low-energy structures (LESs) [9–33]. For the same reason the classical trajectory Monte Carlo method [34–36] is well suited to describe the photoelectron dynamics and has been used to explain the so-called low-energy structures (see, e.g., [11,21,26,37,38]). Although the classical trajectory Monte Carlo simulation can predict the photoelectron momentum distribution, it provides no insight on how the specific features in the momentum distribution emerge.

The quantum descriptions of Coulomb field effects have been implemented using the strong-field approximation (SFA) [39–41] and including Coulomb corrections [42–49]. However, the effect of multiple recollisions is very challenging to treat within SFA [50,51].

In this series of two papers, we develop a classical analytical theory for the description of Coulomb focusing. In the first paper of the series (paper I) we have derived analytical formulas for the Coulomb momentum transfer (CMT) to the electron at the tunnel exit and at recollisions, which are classified as slow or fast recollisions. In this paper (paper II) we calculate analytically the total CMT and derive the final photoelectron momentum distribution while employing these formulas. The advantage of the analytical description is that one can see how the final Coulomb effect is built up during the interaction, and can single out the reason for the appearance of the specific features of the photoelectron momentum distribution. In particular, we have used the analytical approach in paper I to figure out the reason for the counterintuitive energy-dependent shift of the photoelectron momentum cusp in the nondipole regime.

In this paper, we use the previously derived analytical estimates for CMT at recollisions (rec-CMT) and at the tunnel exit (in-CMT) for estimation of the total CMT of any tunneled electrons. For the derivation of the total CMT two analytical methods are applied: fully perturbative and step-by-step method. While in the first method the Coulomb effect is assumed to be a perturbation with respect to the laser driven global electron trajectory, in the second method the Coulomb field is locally treated perturbatively, only near the recollision point; however, the trajectory itself is adjusted after each recollision. We find that CMT is a perturbation with respect to the instantaneous electron momentum at the rescattering; however, it has a nonperturbative contribution with respect to the electron final momentum. Further, we analyze the role of high-order rescattering events in the final CMT.

Once we can derive the total CMT for any tunneled electron, we apply the methods and generate the asymptotic photoelectron momentum distribution. In order to settle the question of whether we can address the Coulomb focusing and its features within our model, we compare the analytically determined spectra to the results of classical trajectory Monte Carlo simulation.

The structure of the paper is the following. In Sec. II, the calculation model of CMT is introduced. Further, the total CMT and the final photoelectron momentum distribution with two methods are derived in Sec. III and the accuracy of our methods is investigated. The conclusion is given in Sec. IV.

*danek@mpi-hd.mpg.de
†k.hatsagortsyan@mpi-hd.mpg.de

 

## II. THE MODEL

We consider the dipole regime of tunneling ionization of an atom in a strong laser field. The laser field is linearly polarized:

$$\mathbf{E}(u) = E_0 \mathbf{e} \cos u, \tag{1}$$

where $u = \omega t$ is the laser phase; $E_0$ and $\omega$ are the amplitude and the angular frequency of the laser field, respectively; and $\mathbf{e} = (1,0,0)$ is the unit vector along the laser polarization direction. We assume that the electron has tunneled out from the atomic bound state which is described by Perelomov, Popov, and Terent'ev (PPT) ionization rate [52]. The initial longitudinal momentum with respect to the laser field direction at the ionization moment $t_i$ is assumed to be vanishing, and the initial coordinate is at the tunnel exit.

Our aim is to find an analytical expression for CMT. We assume that the Coulomb field effect is not negligible only near recollision points and near the tunnel exit, where it is treated as a perturbation with respect to the laser field. The tunnelled electron dynamics in the continuum after tunneling is governed by Newton equations:

$$\frac{d\mathbf{p}}{dt} = -\mathbf{E} - \frac{Z\mathbf{r}}{r^3}, \tag{2}$$

where $\mathbf{p}$ is the electron momentum. Atomic units are used throughout. The Coulomb field of the atomic core will be treated by perturbation theory during the recollision and we expand the momentum and coordinate as

$$\mathbf{p} = \mathbf{p}_0 + \mathbf{p}_1 + \ldots, \quad \mathbf{r} = \mathbf{r}_0 + \mathbf{r}_1 + \ldots. \tag{3}$$

The unperturbed trajectory $\mathbf{r}_0(u)$ is determined by the laser field:

$$\frac{d\mathbf{p}_0}{dt} = -\mathbf{E}, \tag{4}$$

and momentum transfer due to the Coulomb field at the recollision is described by the trajectory in the first order of perturbation:

$$\frac{d\mathbf{p}_1}{dt} = -\frac{Z\mathbf{r}_0}{r_0^3}, \tag{5}$$

with $r_0 = |\mathbf{r}_0|$;

$$\begin{aligned} p_{0x}(u) &= p_{xr} + [A_x(u) - A_x(u_r)], \\ \mathbf{p}_{0\perp}(u) &= \mathbf{p}_{\perp r}, \end{aligned} \tag{6}$$

with the laser vector-potential $A_x(u) = -(E_0/\omega)\sin u$. The initial conditions are defined at the recollision point with the recollision phase $u_r$, and the recollision momentum $\mathbf{p}_r = (p_{xr}, \mathbf{p}_{\perp r})$, aiming at application of the solution near the recollision point. The unperturbed electron trajectory near the recollision point is

$$\begin{aligned} x_0(u) &= \frac{E_0}{\omega^2}[\cos u - \cos u_r + (u - u_r)\sin u_r] \\ &\quad + \frac{p_{xr}}{\omega}(u - u_r) + x_r, \\ \mathbf{r}_{0\perp}(u) &= \frac{\mathbf{p}_{\perp r}}{\omega}(u - u_r) + \mathbf{r}_{\perp r}, \end{aligned} \tag{7}$$

with the recollision coordinate $\mathbf{r}_r = (x_r, \mathbf{r}_{\perp r})$.

Once the zeroth-order equations are solved, the momentum transfer due to the Coulomb field at the recollision can be derived as the first-order correction

$$\mathbf{p}_1 = -\frac{Z}{\omega}\int_{u_r-\delta}^{u_r+\delta} \frac{\mathbf{r}_0(u')}{r_0^3(u')} du', \tag{8}$$

where $\mathbf{r}_0(u) = (x_0(u), \mathbf{r}_{0\perp}(u))$. The value of the parameter $\delta$ is coupled to the properties of the recollision and is discussed in Sec. III of paper I, where we also present analytical solutions to Eq. (8) for the well-defined recollision events.

In the discussion above, the Coulomb field effect is accounted for only near recollision points and near the tunnel exit, where it is treated as a perturbation with respect to the laser field. Still Eq. (8) for CMT includes nonperturbative Coulomb effects via dependence on the recollision parameters, i.e., the electron momentum $\mathbf{p}_r$ and coordinate $\mathbf{r}_r$ at the recollision point. The role of multiple recollisions for the total momentum transfer is discussed in Sec. III.

One may also apply a less accurate description assuming that the Coulomb field is a perturbation globally, i.e, at any moment the difference between the exact and laser driven trajectories is small and negligible. In this description the unperturbed electron trajectory is given by Eqs. (6), replacing the recollision phase $u_r$ by the ionization phase $u_i$, and replacing the recollision coordinate $\mathbf{r}_r$ and momentum $\mathbf{p}_r$ by the coordinate and momentum at the tunnel exit: $\mathbf{r}_i = (x_i, 0, 0)$ and $\mathbf{p}_i = (0, p_{yi}, p_{zi})$, respectively. The tunnel exit can be roughly estimated in the quasistatic regime as $x_i = -I_p/E(u_i)$, which corresponds to the zero-range potential case.

## III. TOTAL MOMENTUM TRANSFER AND PHOTOELECTRON MOMENTUM DISTRIBUTION

In this section, we illustrate the capability of our analytical approach to provide an estimation of the final momenta for any arbitrary ionization phase $u_i$, and initial transversal momentum $p_{\perp i}$ and, accordingly, the estimation for the asymptotic photoelectron momentum distribution. We compare our analytical results with the numerical classical trajectory Monte Carlo simulations, to check whether the derived analytical formulas for rec-CMT and in-CMT can provide physically relevant results. We consider two different approaches: the straightforward zeroth-order trajectory approach and the more elaborate step-by-step approach. For simplicity the dipole approximation is applied and $I_p = 0.5$ and $Z = 1$ throughout this section.

### A. Zeroth-order trajectory approach

In this approach, the Coulomb field of the atomic core is treated as a global perturbation. Then, the zeroth-order trajectory describes the trajectory of the electron solely in the laser field. The total Coulomb effect mostly amounts to in-CMT and rec-CMT (there is also a small asymptotic contribution after the laser pulse is switched off, which was discussed in paper I. For the estimation of rec-CMT, we use the zeroth-order trajectory to find the rescattering points and for each rescattering event apply our rec-CMT formulas derived in Sec. III of paper I. The in-CMT distorts the zeroth-order trajectory significantly, which can have an essential impact on the rescattering points. Therefore, we include the in-CMT

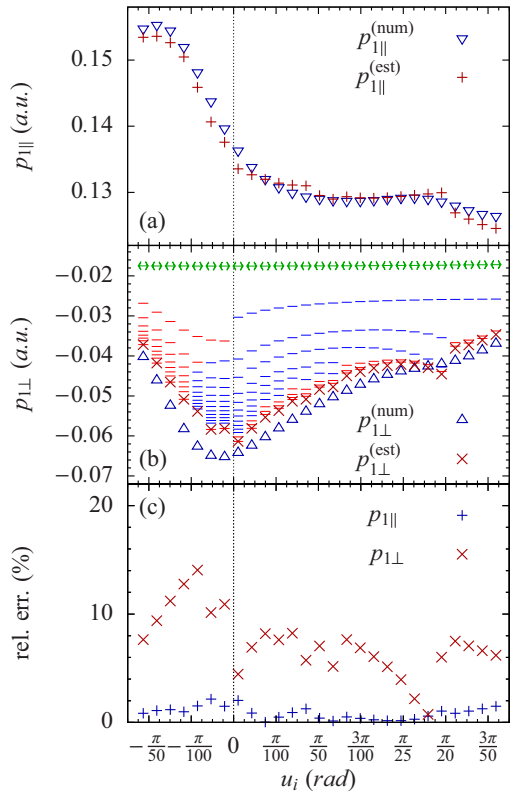


FIG. 1. Total CMT vs ionization phase $u_i$ via the zeroth-order trajectory approach: (a) longitudinal momentum transfer, (b) transverse momentum transfer, and (c) the corresponding errors; $p_{\perp i} = 0.2$. Numerical simulations are shown with triangles, the estimation (see the text) is shown with red crosses, and in-CMT is shown with a green double arrow. The contribution of each rec-CMT is shown by a line segment: slow recollision, red; fast recollision, blue. The contributions are added to in-CMT and to the previous rec-CMTs, as long as it is larger than 5% of the total numerical estimate of CMT. This restriction was applied for the sake of graphical simplicity only.

in the zeroth-order trajectory via modification of the initial momentum (see Appendix A1).

We compare results of our analytical estimations for the total momentum transfer with numerical simulations in Fig. 1 (in the latter a smooth switch-off of the laser pulse is used). For $u_i > 0$, a very good agreement with the numerical simulations is achieved. The error is well behaved and peaks at the phases where two methods are switching, namely, the single slow recollision forks into two fast recollisions. There is an easily understandable discrepancy for $u_i < 0$, since decreasing $u_i$ tilts the electron's quivering trajectory down and hence the first recollision becomes slow, which generally yields larger momentum transfer than fast recollision. For some particularly small and especially negative $u_i$, the momentum transfer is so large that the whole zeroth-order trajectory is not a valid approximation anymore and our present approach fails. The accuracy issue will be discussed below in Sec. III D.

We underline an important message of Fig. 1, which has been enabled by our analytical approach. A single rescattering is not sufficient to describe the CMT. The contribution of high-order rescatterings to the total CMT is significant and should not be neglected for a good quantitative description.

### B. Step-by-step approach

When the electron is ionized near the peak of the laser field, its drift velocity is small, and rescattering can happen with a small impact parameter, inducing large distortion of the laser driven trajectory. The same can happen when the electron is ionized with a small transverse momentum at other ionization phases. It is understandable that the zeroth-order approximation fails in this case. However, we can improve our estimations by taking into account rec-CMT at each recollision during propagation in the laser field. Thus, the electron is propagated by the laser field only step by step from the ionization phase $u_i$ till the end of the laser pulse over all the rescattering events, and by correcting the electron momentum by the estimated rec-CMT at every single recollision point. This approach is expected to give much more precise results, with a wider range of applicability of ionization phases and initial transverse momenta.

Although the laser driven trajectory is disturbed due to rec-CMT at the recollisions, the rec-CMT itself can be still calculated using perturbation theory because the latter is always applicable at least during the short time of the recollision. This allows us to use the same formulas for rec-CMT as in the previous subsection. The only difference is that the zeroth-order trajectory is replaced by several step-by-step evolved zeroth-order trajectories (for more details see Appendix A2).

We plotted the resulting CMT for various ionization phases and fixed $p_{\perp i} = 0.2$ a.u. in Fig. 2. The relative error does not change much for the positive phases where only few rescatterings take place. For the negative phases we can actually see an increase in the precision which is a good indication that our step-by-step approach could deliver much better results.

Although the procedure of finding the right rescattering points seems to be straightforward, we need a quite good algorithm selecting them automatically in order to automatize the methods. The algorithms for selection of the proper rescattering point can be found in Appendix B.

We point out the remarkable qualitative similarity of the results of the two methods for the total CMT in Figs. 1 and 2. Although the zeroth-order trajectory approach is less accurate quantitatively [see the larger error for $p_{1\parallel}$ at $u_i < 0$ in Fig. 1(c) with respect to Fig. 2(c)], the behavior of the transverse and longitudinal rec-CMT with respect to the laser phase is similar. Both methods show that the contribution of high-order rescatterings to the total CMT is significant and determines the behavior of the total CMT with respect to the ionization phase.

### C. Comparing methods

Let us compare the accuracy of both methods over the whole valid parameter space. For a special class of initial conditions, the components of the final momentum can be vanishing, leading to an artificial enhancement of the relative error. Therefore, we redefine the relative error as follows:

$$\delta p_\parallel = \left| \frac{p_\parallel(u_i, p_{\perp i}) - p_\parallel^{(num)}(u_i, p_{\perp i})}{\max\left[p_\parallel(u_i, p_{\perp i}), p_\parallel(u_i, p_{\perp i}) - p_{0\parallel}(u_i)\right]} \right| 100\%, \quad (9)$$

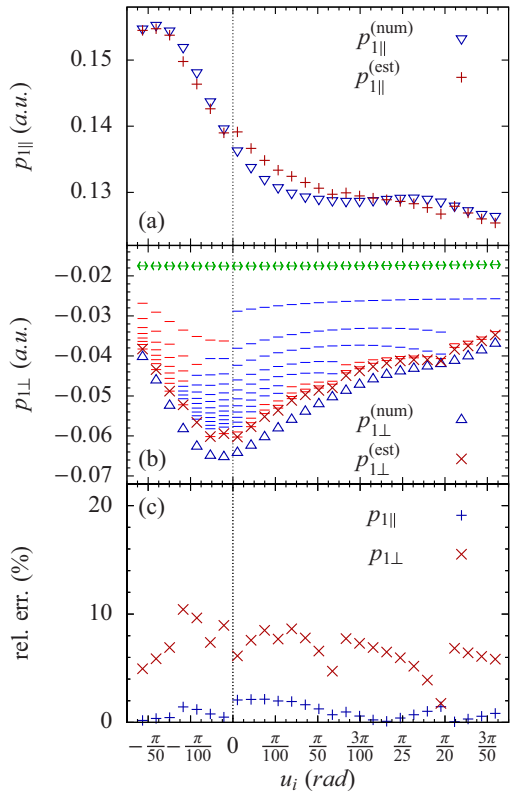


FIG. 2. Total CMT vs ionization phase $u_i$ via the step-by-step approach: (a) longitudinal momentum transfer, (b) transverse momentum transfer, and (c) the corresponding errors; $p_{\perp i} = 0.2$. Numerical simulations are shown with triangles, the estimation (see the text) is shown with red crosses, and in-CMT is shown with a green double arrow. The contribution of each rec-CMT is shown by a line segment: slow recollision, red; fast recollision, blue. The contributions are added to in-CMT and to the previous rec-CMTs, as long as it is larger than 5% of the total numerical estimate for CMT, again, for the sake of clarity only.

$$\delta p_\perp = \left| \frac{p_\perp(u_i, p_{\perp i}) - p_\perp^{(\mathrm{num})}(u_i, p_{\perp i})}{\max\left[p_\perp(u_i, p_{\perp i}), p_\perp(u_i, p_{\perp i}) - p_{0\perp}(u_i)\right]} \right| 100\%, \tag{10}$$

with $p_{\parallel/\perp}(u_i, p_{\perp i})$ being the proper component of the electron's final momentum given by Eq. (A4) or by Eq. (A5) at $n = N$ for the zeroth-order or step-by-step method, respectively. The superscript "(num)" denotes the corresponding value obtained numerically and subscript "0" marks the value obtained from the zeroth-order trajectory neglecting any Coulomb interaction. The newly defined relative error is well behaved even for the final vanishing momentum where the momentum is replaced with the total CMT instead. We show the redefined error for valid ranges of the ionization phase $u_i$, and the initial transversal momentum in Fig. 3 for our zeroth-order trajectory method and in Fig. 4 for the step-by-step method.

Obviously, the initial momentum $p_{\perp i}$ plays a crucial role. With decreasing $p_{\perp i}$ the first rescattering has a smaller impact parameter and, therefore, induces larger CMT, which will introduce discrepancy to the zeroth-order trajectory. Thus, our

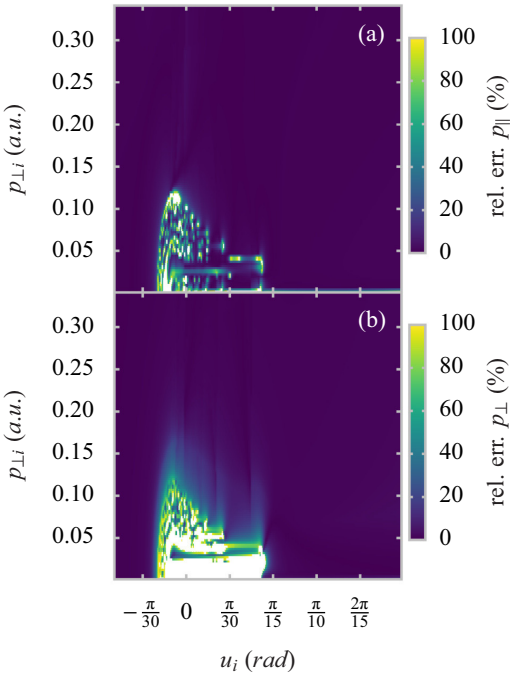


FIG. 3. Relative error of the photoelectron estimated asymptotic momentum in the zeroth-order trajectory approach: (a) longitudinal momentum and (b) transverse momentum.

method for analytical estimation of CMT is not applicable for small initial transverse momenta of the ionized electron and for small ionization phases (near the peak of the laser field). The vertical lobes indicate the ionization phases with underlying slow recollision. The error rises there, since the CMT at such

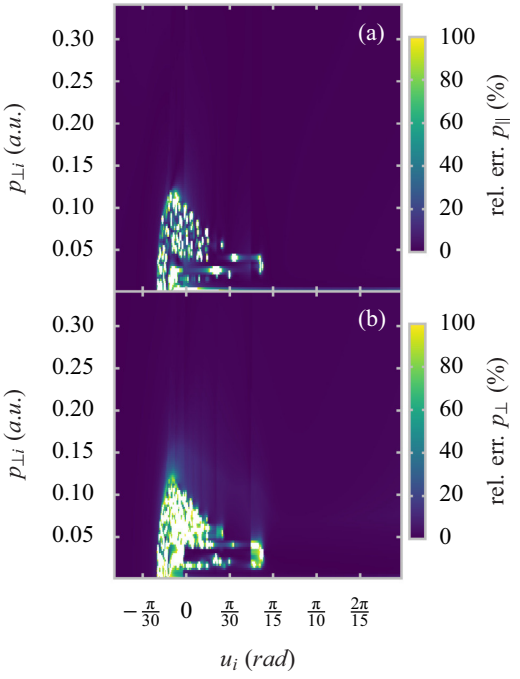


FIG. 4. Relative error of the photoelectron estimated asymptotic momentum in the step-by-step approach: (a) longitudinal momentum and (b) transverse momentum.

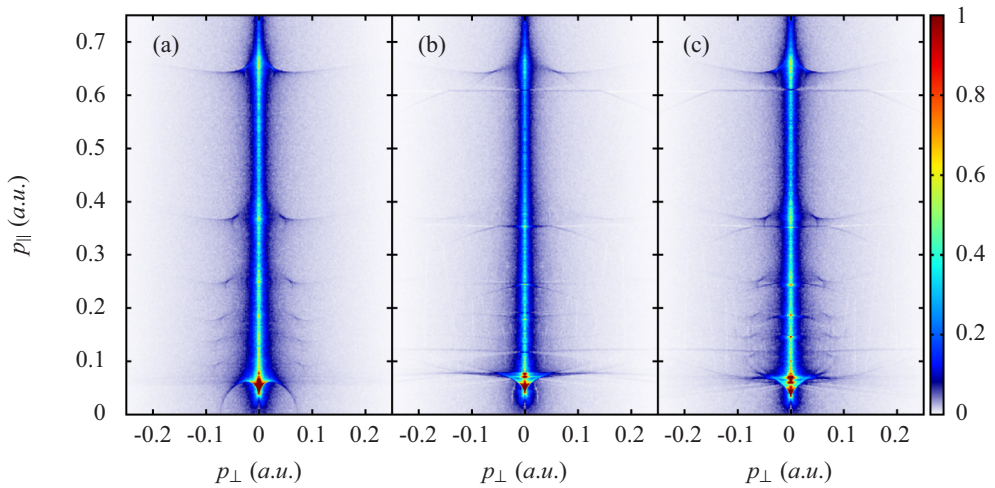


FIG. 5. Photoelectron momentum distribution: (a) numerical classical trajectory Monte Carlo simulation, (b) via the zeroth-order trajectory method, and (c) via the step-by-step method.

recollision is much larger than the CMT at fast recollisions and even a small relative error has a large total contribution.

Finally, let us note that the white areas arise due to several effects, such as chaotic dynamics, hard recollisions, and the trapping of electrons in Rydberg states. Such effects do not play a significant role for Coulomb focusing. The role of the errors of the present analytical approach for the description of the final photoelectron momentum distribution is discussed in the next section.

### D. Photoelectron momentum distribution

In the previous subsection, we have seen that our analytical methods allow us to determine the photoelectron asymptotic momentum during the laser driven excursion in the continuum in the field of the atomic core. However, since the accuracy is not acceptable in the whole range of the ionization phases or in the initial transverse momenta, a question arises, namely, how accurately can the final photoelectron momentum distribution be described by our methods? In this section we compare results of fully numerical classical trajectory Monte Carlo simulation of the final photoelectron momentum distribution with those of our analytical methods. In order to do this, we performed classical trajectory Monte Carlo simulations in two dimensions due to the symmetry of the problem in the dipole approximation. Every two-dimensional (2D) trajectory of the initial transversal momentum $p_{\perp i}$ is weighted with the PPT transverse momentum distribution $w_{\mathrm{PPT}}(p_{\perp i})$ and with an additional factor of $2\pi p_{\perp i}$. The latter accounts for the fully three-dimensional (3D) initial phase space the two transversal dimensions of which can be mapped onto a single dimension due to the symmetry via $d^2p_{\perp i} = 2\pi p_{\perp i} dp_{\perp i}$. With the electron asymptotic distribution function $w_{\mathrm{sim}}(p_\parallel, p_\perp)$ provided by the 2D classical trajectory Monte Carlo simulation, one restores the real final 3D photoelectron momentum distribution:

$$\frac{d^3f}{d^3p} \propto \frac{w_{\mathrm{sim}}(p_\parallel, p_\perp)}{2\pi p_\perp}, \tag{11}$$

where we have restored the second transversal dimension via the relation $d^2p_\perp = 2\pi p_\perp dp_\perp$ for the final transversal momentum $p_\perp$.

We performed three different classical trajectory Monte Carlo simulations with $10^7$ trajectories to determine the photoelectron momentum distribution at the end of the laser pulse: one fully numerical, the second using our zeroth-order trajectory method, and the last using the step-by-step method. The resulting photoelectron momentum distributions are compared in Fig. 5.

As we can see, both methods reproduce the central vertical cusp. However, the width of the cusp is reproduced by the step-by-step method more correctly. On one hand, the horizontal fringes appear already by the zeroth-order method, which can be understood as a manifestation of the fine role of the slow recollisions (so-called longitudinal bunching [25]). On the other hand, the step-by-step method seems to reconstruct even the right thickness and location of the fringes and thus we conclude it is a better investigative tool. Unfortunately, both simulated photoelectron momentum distributions exhibit additional horizontal lines (e.g., at $p_x \approx 0.61$ a.u.). Such lines can be attributed to an "artificial" longitudinal bunching effect which arises when one slow recollision is replaced by two fast recollisions yielding a slightly greater total CMT. Because of this artifact, an additional horizontal line appears underneath each slow recollision regular fringe, which is demonstrated as a twofold line in the photoelectron momentum distributions. Luckily, the utility of the results is not jeopardized since the artificial fringe is much weaker than the real effect and can be therefore easily disclosed.

The numerical photoelectron momentum distribution possesses a half-circle fringe of radius ~0.08 a.u. (center at the origin) with a prominent peak structure inside. This structure is created by electrons with low transverse momenta near the peak of the laser pulse, for which the error of our analytical methods is large (see white areas in Figs. 3 and 4). Although both analytical methods reproduce the peak, they fail to predict the correct structure of it. This is due to the fact that these electrons undergo multiple recollisions with large CMT and

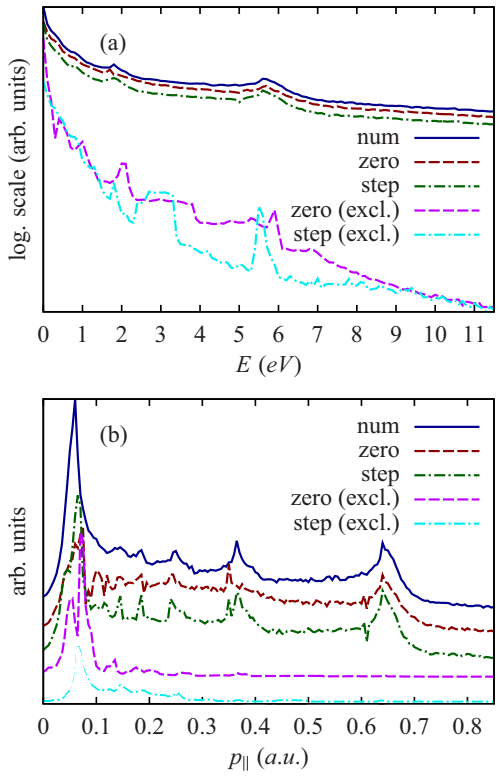


FIG. 6. (a) Photoelectron energy distribution. (b) Photoelectron longitudinal momentum distribution: numerical classical trajectory Monte Carlo simulation (solid, blue), via the zeroth-order trajectory method (dashed, red), and via the step-by-step method (dash-dotted, green). We show also distributions while restricting trajectories to those with an error greater than 100% in at least one direction: via the zeroth-order trajectory method (dashed, magenta) and via the step-by-step method (dash-dotted, cyan). The curves are shifted vertically for visibility while keeping the same shift for the same methods in individual panels.

never really gain substantial distance from the ion during the whole laser pulse and are strongly influenced by the Coulomb field even when the pulse is long gone. For such behavior, the perturbative recollision picture does not hold and our methods fail.

Since LES was first observed in the photoelectron energy spectra [9], we investigated in Fig. 6(a) whether they can be reproduced by our analytical methods. The spectrum and the longitudinal momentum distribution [in Fig. 6(b)] are obtained by the classical trajectory Monte Carlo simulations where we separated the contributions of the electrons with their total CMT estimated with errors smaller than 100% and of the remaining electrons with their total CMT estimated more wrongly. As we see, the excluded contributions of the wrongly estimated photoelectrons are negligible in the energy domain, especially for nonvanishing energies. However, a sharp peak can be found at $p_x \approx 0.075$ a.u., which can be discerned clearly in Fig. 6(b). As we can see, already the zeroth-order trajectory method captures the positions of the peaks in the energy distribution Fig. 6(a) quite correctly. Nevertheless, the peak at the vanishing longitudinal momentum is misplaced, which is corrected by the more precise step-by-step method.

We can conclude that our analytical approach is able to predict correctly many features of photoelectron momentum distribution, in particular, width of the vertical cusp, the peaks along it, and the position of the horizontal caustic fringes due to the longitudinal bunching. Our approach fails only at very low momenta $p_x \lesssim 0.05$ a.u. While predicting the existence of the lowest momentum peak, none of our methods provides its correct structure. The reason is that the trajectories with a large error (white areas in Figs. 3 and 4) mostly contribute to this prominent peak at low momenta, which explains the noticeable discrepancy between the numerics and our results in this region. On the bright side, the white areas contribute to the momentum peaks at larger energies only negligibly and do not threaten the utility of our approach to Coulomb focusing for the largest part of the photoelectron momentum distribution [see Fig. 6(b)].

## IV. CONCLUSION

We have developed an analytical description of Coulomb focusing effects in laser induced strong-field ionization, which is based on the analytical formulas for CMT derived in paper I. For the derivation, the Coulomb field effect is treated as a perturbation at recollisions.

In paper II, we used the analytical formulas for CMT at the tunnel exit and later at the rescattering events from paper I in order to derive the total CMT on an electron tunneled at any arbitrary ionization phase. For this purpose, we proposed two different methods which we also successfully applied for derivation of the final photoelectron momentum distributions.

Besides the simplest zeroth-order laser driven trajectory method, we put forward also the step-by-step method, when after each recollision the electron trajectory is corrected accounting for CMT at the recollision. We show that the accuracy of our approach fails only at very low photoelectron energies. In addition, the latter method provides an extension of the model beyond the perturbative regime, where the CMT at a recollision introduces significant distortion to the global trajectory, and leads to a better agreement with numerical simulations at low photoelectron energies than the former method.

The perturbative treatment of the Coulomb field effect was successfully applied for investigation of Coulomb focusing and its features. We found out that the treatment is well suited for the description of the Coulomb focusing as it arises due to multiple forward scatterings of the ionized electrons by the atomic core at relatively large impact parameters. Nevertheless, the perturbative treatment seems to fail for recollisions with small impact parameter leading to well-known processes of above-threshold ionization. During these hard recollisions, the electron absorbs a large amount of energy from the laser and finally ends up at high energies. However, the contribution of the hard recolliding trajectories to the Coulomb focusing cusps is minor.

The analytical description of Coulomb focusing allows estimation of the role of each particular rescattering event. In particular, we have proven by our analytical approach (see Fig. 2) that single rescattering is not sufficient to quantitatively describe Coulomb focusing in midinfrared laser fields and the contribution of high-order rescatterings should not be neglected.

## APPENDIX A: THE TOTAL CMT

In this section we define two methods for derivation of the total CMT: the zeroth-order method and the step-by-step method.

### 1. Zeroth-order trajectory approach

In this approach, the Coulomb field of the atomic core is treated as a global perturbation. The zeroth-order trajectory describes the electron in the laser field:

$$\tilde{x}_0(u) = \frac{E_0}{\omega^2}[\cos u - \cos u_i + (u-u_i)\sin u_i] + (u-u_i)\frac{p_{2\parallel,\mathrm{in}}}{\omega} + x_i, \tag{A1}$$

$$\tilde{y}_0(u) = \frac{p_{yi} + p_{2y,\mathrm{in}}}{\omega}(u-u_i), \tag{A2}$$

$$\tilde{z}_0(u) = \frac{p_{zi} + p_{2z,\mathrm{in}}}{\omega}(u-u_i), \tag{A3}$$

with $p_{2y,\mathrm{in}}$ and $p_{2z,\mathrm{in}}$ being projections of the transversal in-CMT $p_{2\perp,\mathrm{in}}(u_i, \sqrt{p_{yi}^2 + p_{zi}^2})$ in $y$ and $z$ directions, respectively. The in-CMT $p_{2\parallel,\mathrm{in}}$ and $p_{2\perp,\mathrm{in}}$ are given in paper I by Eqs. (36) and (37), respectively.

The final momentum is obtained by including the contribution of all rec-CMT into the momentum transfer, yielding

$$\mathbf{p}(u_i,\mathbf{p}_{\perp i}) = \mathbf{p}_0(u_i,\mathbf{p}_{\perp i}) + \mathbf{p}_{2,\mathrm{in}}(u_i,\mathbf{p}_{\perp i}) + \sum_{j=1}^{N} \mathbf{p}_1^{(j)}(u_i,\widetilde{\mathbf{p}}_{\perp i}), \tag{A4}$$

where $N$ is the total number of effective rescatterings, $\mathbf{p}_0(u_i) = (-A(u_i), p_{yi}, p_{zi})$ is the zeroth-order asymptotic momentum, $\mathbf{p}_{\perp i} = (0, p_{yi}, p_{zi})$ is the initial transverse momentum, $\mathbf{p}_{2,\mathrm{in}}(u_i,\mathbf{p}_{\perp i}) \equiv p_{2\parallel,\mathrm{in}}(u_i,|\mathbf{p}_{\perp i}|)\mathbf{e} - |p_{2\perp,\mathrm{in}}(u_i,|\mathbf{p}_{\perp i}|)|\frac{\mathbf{p}_{\perp i}}{|\mathbf{p}_{\perp i}|}$ is the initial momentum correction, $\widetilde{\mathbf{p}}_{\perp i} \equiv \mathbf{p}_{\perp i} - |p_{2\perp,\mathrm{in}}(u_i,|\mathbf{p}_{\perp i}|)|\frac{\mathbf{p}_{\perp i}}{|\mathbf{p}_{\perp i}|}$ is the distorted initial transversal momentum, and $\mathbf{p}_1^{(j)}(u_i,\widetilde{\mathbf{p}}_{\perp i})$ is the rec-CMT at $j$th recollision given by the formulas derived in paper I, corresponding to the specific type of this recollision.

We treat a recollision as slow recollision, when $\dot{x}_r = 0$ and $x_r\ddot{x}_r > 0$, as well as those when $\dot{x}_r = 0$, $x_r\ddot{x}_r < 0$, but only as long as $|x_r| < x_{\mathrm{thresh}} = E_0/(5\omega^2)$. For the estimation of rec-CMT we use Eqs. (A1)–(A3) from paper I in both cases. All slow recollisions with $|\ddot{x}_r| < \ddot{x}_{\mathrm{thresh}} = E_0/10$ are neglected because such recollisions happen at the end of the laser pulse and have negligible rec-CMT (see Fig. 7). For some electrons this is not true, however most of them are further trapped in the Rydberg states.

Finally, we treat the remaining rescatterings as fast recollision and use the estimates given in paper I by Eqs. (23)–(25) or Eqs. (B7)–(B9), depending on the conditions given by Eqs. (B10) and (B11). The only exceptions are the fast recollision closest to any slow recollision with $x_r\ddot{x}_r < 0$ and $|x_r| < x_{\mathrm{thresh}}$, which we neglect since the rec-CMT is already taken into account via the slow recollision (see an exemplary slow recollision at $u_r \sim 2\pi$ or $13\pi$ replacing the two closest fast recollisions in Fig. 7).

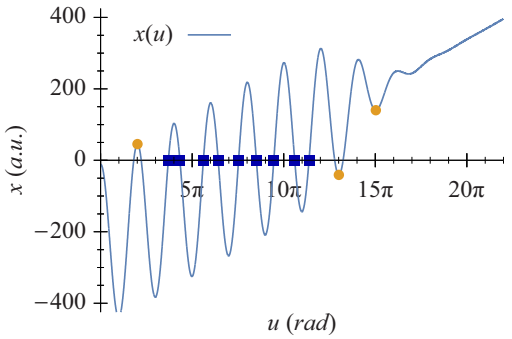


FIG. 7. An illustrative trajectory demonstrating two different types of recollisions: slow recollision (by orange dots) and fast recollision (by blue squares). We keep the slow recollision points if $|x_r| < E_0/(5\omega^2)$ for $x_r\ddot{x}_r < 0$, otherwise we find the closest fast recollision points. We also keep those slow recollisions with $x_r\ddot{x}_r > 0$ but neglect any slow recollision points with $\ddot{x}_r < E_0/10$.

### 2. Step-by-step approach

In this approach the electron is propagated by the laser field only step by step from the ionization phase $u_i$ till the end of the laser pulse over all the rescattering events, and by correcting the electron momentum by the estimated rec-CMT at every single recollision point.

The drift momentum after the $n$th recollision is dependent of all rec-CMT received at all previous recollisions and can be iteratively defined as

$$\mathbf{p}^{(n)}(u_i,\mathbf{p}_{\perp i}) = \mathbf{p}^{(n-1)}(u_i,\mathbf{p}_{\perp i}) + \mathbf{p}_1^{(n)}(u_i,\mathbf{p}^{(n-1)}(u_i,\mathbf{p}_{\perp i})), \tag{A5}$$

where we have for simplicity redefined the in-CMT as zeroth-order rec-CMT: $\mathbf{p}_1^{(0)}(u_i,\mathbf{p}_{\perp i}) \equiv p_{2\parallel,\mathrm{in}}(u_i,|\mathbf{p}_{\perp i}|)\mathbf{e} - |p_{2\perp,\mathrm{in}}(u_i,|\mathbf{p}_{\perp i}|)|\frac{\mathbf{p}_{\perp i}}{|\mathbf{p}_{\perp i}|}$. The iteration starts at $n = -1$ with $\mathbf{p}^{(-1)}(u_i,p_{\perp i}) := -A_x(u_i)\mathbf{e} + \mathbf{p}_{\perp i}$. Let us note that $n = 0$ corresponds to the momentum after tunneling and before the first rescattering event which happens at $n = 1$. The properties of the $n$th rescattering can be determined from the zeroth-order trajectory evolved from the $(n-1)$th event with the $\mathbf{p}^{(n-1)}(u_i,p_{\perp i})$ momentum yielding

$$x_0^{(n)}(u) = \frac{1}{\omega}\int_{u_{in}}^{u} \left(p_x^{(n)}(u_i,p_{\perp i}) + A_x(u)\right)du + x_0^{(n-1)}(u_{in}), \tag{A6}$$

$$\mathbf{r}_{0\perp}^{(n)}(u) = \mathbf{p}_{\perp i}^{(n)}(u_i,p_{\perp i})\left(\frac{u-u_{in}}{\omega}\right) + \mathbf{r}_{0\perp}^{(n-1)}(u_{in}), \tag{A7}$$

where we set $u_{in} = u_r$ of the $n$th rescattering. The tunnel exit enters the iteration as $x_0^{(-1)} = x_i$, $\mathbf{r}_{0\perp}^{(-1)} = (0,0)$, and for $n = 0$ we have $u_{in} = u_i$.

Trajectories obtained with the step-by-step and the zeroth-order approaches are compared with the numerical simulation for $u_i = -\pi/100$ in Fig. 8. As we can see, the trajectories do not differ for the first half period which is achieved by taking the initial momentum correction into account. The difference starts to manifest during the second half period of the laser field (i.e., after the first rescattering); however, the step-by-step

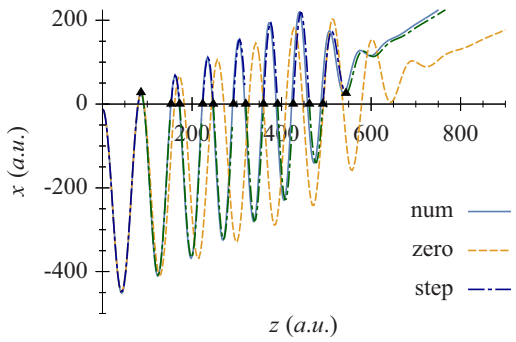


FIG. 8. The electron trajectories in different approaches: (solid, gray) numerical solution, (dashed, orange) zeroth-order approach, and (dot-dashed, multicolor) step-by-step approach. Rescattering points are noted by black triangles. All trajectories match well for the first half period but start to differ after the first rescattering event. The used parameters are $E_0 = 0.041$, $\omega = 0.0134$, $u_i = -\pi/100$, and $p_{\perp i} = 0.2$.

zeroth-order trajectory approach provides a rather good approximation for the exact numerical trajectory.

## APPENDIX B: METHODS

Despite the precise method we use, the essence of our semianalytical approach is the correct determination of the rescattering points. The main challenge is to find an algorithm that will correctly choose the rescattering points and refuse other candidates. Even though the underlying principles for the rescattering point classification are the same, differences can be found and both methods require special algorithms. Let us therefore discuss the methods separately.

### 1. Zeroth-order trajectory

Since we know the whole zeroth-order trajectory distorted by the in-CMT analytically from Eqs. (A1)–(A3), we can easily determine the rescattering points as $p_{0\|}(u_r) + p_{1\|,\mathrm{in}} = 0$ for slow rescattering (save them in sorted list S) and $\tilde{x}_0(u_r) = 0$ for fast cases (and save them in sorted list F) up to the end of the laser pulse. The lists are sorted increasingly with respect to the rescattering phase $u_r$ of the individual events. The number of elements in a list will be denoted by prefix "#." Once we have gathered all the candidates, we have to apply selection rules.

(1) Remove the first element in S if its rescattering phase $u_r \sim \pi$.

(2) When #F $> 1$: starting from the lowest $u_r$, for each neighboring pair of F points find the S recollision they surround if its distance $|x(u_r)| > x_{\mathrm{thresh}}$, otherwise memorize the two F points for later removal; finally, after analyzing of all F pairs remove all memorized F points.

(3) From the S rescatterings we keep only those fulfilling one of the following two conditions:

$$\mathbf{r}(u_r)\cdot\mathbf{E}(u_r) > 0 \quad \text{and} \quad |x(u_r)| < x_{\mathrm{thresh}}, \tag{B1}$$

$$\mathbf{r}(u_r)\cdot\mathbf{E}(u_r) < 0 \quad \text{and} \quad |\mathbf{E}(u_r)| > E_{\mathrm{thresh}}, \tag{B2}$$

where the first condition selects all the unfavorable turning points when they happen close enough to the ion and the second condition selects all the favorable turning points excluding those at the end of the laser pulse with respect to the thresh $E_{\mathrm{thresh}}$.

Let us note that the end of the pulse must be chosen approximately because otherwise fast recollisions could appear for late phases when the quiver motion is nearly non-existing. For such recollisions we lack estimations of rec-CMT but their contribution to the total momentum is assumed to be vanishing due to the large distance from the ion for trajectories of our interest.

### 2. Step-by-step approach

The step-by-step method is a little bit more elaborated and the general scheme from the zeroth-order trajectory cannot be used. Since we are interested only in the next rescattering point, there is little sense in searching for all the rescattering points till the end of the laser pulse in order to find the proper subsequent one.

Therefore, we find all the slow or fast candidates within the range $u_r < 9\pi/4 + u_{in}$ with $u_{in} = u_i$ and $n = 0$ by using the zeroth-order vector Eq. (A5) and we find the step-by-step evolved trajectory by Eqs. (A6) and (A7) in complete analogy to the zeroth-order case, prepending the ionization phase to the list F and apply the following procedure.

(1) If #S + #F $= 1$ there are no further rescattering points.

(2) If the first event in F precedes the first event in S: remove the first element in S if its $u_r < \pi + u_{in}$.

(3) If the first element in S precedes the first element in F, (a) remove the second element in S if its $u_r < \pi/4 + u_{in}$ (eliminating fake slow recollision due to non-negligible rec-CMT); (b) if #F $> 0$ then remove the first element in F when its $u_r < \pi + u_{in}$, otherwise remove every even element in S or every element in S for which $|\mathbf{E}(u_r)| < E_{\mathrm{thresh}}$—the remaining list S contains all valid rescattering points.

(4) When #F $> 1$: starting from the lowest $u_r$, for each neighboring pair of F points find the S recollision they surround if its distance $|x(u_r)| > x_{\mathrm{thresh}}$, otherwise memorize the two F points for later removal; finally, after analyzing of all F pairs remove all memorized F points.

(5) From the S rescatterings we keep only those fulfilling one of the following two conditions:

$$\mathbf{r}(u_r)\cdot\mathbf{E}(u_r) > 0 \quad \text{and} \quad |x(u_r)| < x_{\mathrm{thresh}}, \tag{B3}$$

$$\mathbf{r}(u_r)\cdot\mathbf{E}(u_r) < 0 \quad \text{and} \quad |\mathbf{E}(u_r)| > E_{\mathrm{thresh}}, \tag{B4}$$

where the first condition selects all the unfavorable turning points when they happen close enough to the ion and the second condition selects all the favorable turning points excluding those at the end of the laser pulse with respect to the thresh $E_{\mathrm{thresh}}$.

At the end of this procedure, we have a list of all valid rescattering points including the original one. The second element of the union S + F is the next rescattering point and we can estimate the momentum after this rescattering from Eqs. (A5) by using the right rescattering type and formula. Now we set $u_{in} = u_r$ and clear the lists S, F; further, we append the

rescattering point $u_r$ to the proper list instead of the ionization phase and repeat the whole procedure above for $n = n + 1$. We repeat so till no further rescattering points are found (i.e., $\#S + \#F = 1$) or until the end of the laser pulse. Again, there is some caution required while setting the end of the pulse in order to eliminate the unwanted fast recollisions.


[1] P. B. Corkum, Phys. Rev. Lett. **71**, 1994 (1993).
[2] W. Becker, F. Grasbon, R. Kopold, D. B. Milošević, G. G. Paulus, and H. Walther, Adv. At. Mol. Opt. Phys. **48**, 35 (2002).
[3] P. Agostini and L. F. DiMauro, Rep. Prog. Phys. **67**, 813 (2004).
[4] W. Becker, X. Liu, P. J. Ho, and J. H. Eberly, Rev. Mod. Phys. **84**, 1011 (2012).
[5] T. Brabec, M. Y. Ivanov, and P. B. Corkum, Phys. Rev. A **54**, R2551 (1996).
[6] G. L. Yudin and M. Y. Ivanov, Phys. Rev. A **63**, 033404 (2001).
[7] D. Comtois, D. Zeidler, H. Pépin, J. C. Kieffer, D. M. Villeneuve, and P. B. Corkum, J. Phys. B **38**, 1923 (2005).
[8] B. Wolter, M. G. Pullen, M. Baudisch, M. Sclafani, M. Hemmer, A. Senftleben, C. D. Schröter, J. Ullrich, R. Moshammer, and J. Biegert, Phys. Rev. X **5**, 021034 (2015).
[9] C. I. Blaga, F. Catoire, P. Colosimo, G. G. Paulus, H. G. Muller, P. Agostini, and L. F. DiMauro, Nat. Phys. **5**, 335 (2009).
[10] F. Catoire, C. Blaga, E. Sistrunk, H. Muller, P. Agostini, and L. DiMauro, Laser Physics **19**, 1574 (2009).
[11] W. Quan, Z. Lin, M. Wu, H. Kang, H. Liu, X. Liu, J. Chen, J. Liu, X. T. He, S. G. Chen, H. Xiong, L. Guo, H. Xu, Y. Fu, Y. Cheng, and Z. Z. Xu, Phys. Rev. Lett. **103**, 093001 (2009).
[12] C. Y. Wu, Y. D. Yang, Y. Q. Liu, Q. H. Gong, M. Y. Wu, X. Liu, X. L. Hao, W. D. Li, X. T. He, and J. Chen, Phys. Rev. Lett. **109**, 043001 (2012).
[13] B. Wolter, C. Lemell, M. Baudisch, M. G. Pullen, X.-M. Tong, M. Hemmer, A. Senftleben, C. D. Schröter, J. Ullrich, R. Moshammer, J. Biegert, and J. Burgdörfer, Phys. Rev. A **90**, 063424 (2014).
[14] J. Dura, N. Camus, A. Thai, A. Britz, M. Hemmer, M. Baudisch, A. Senftleben, C. D. Schröter, J. Ullrich, R. Moshammer, and J. Biegert, Sci. Rep. **3**, 2675 (2013).
[15] M. G. Pullen, J. Dura, B. Wolter, M. Baudisch, M. Hemmer, N. Camus, A. Senftleben, C. D. Schröter, R. Moshammer, J. Ullrich, and J. Biegert, J. Phys. B **47**, 204010 (2014).
[16] Q. Z. Xia, D. F. Ye, L. B. Fu, X. Y. Han, and J. Liu, Sci. Rep. **5**, 11473 (2015).
[17] K. Zhang, Y. H. Lai, E. Diesen, B. E. Schmidt, C. I. Blaga, J. Xu, T. T. Gorman, F. Légaré, U. Saalmann, P. Agostini, J. M. Rost, and L. F. DiMauro, Phys. Rev. A **93**, 021403 (2016).
[18] E. Diesen, U. Saalmann, M. Richter, M. Kunitski, R. Dörner, and J. M. Rost, Phys. Rev. Lett. **116**, 143006 (2016).
[19] J. B. Williams, U. Saalmann, F. Trinter, M. S. Schöffler, M. Weller, P. Burzynski, C. Goihl, K. Henrichs, C. Janke, B. Griffin, G. Kastirke, J. Neff, M. Pitzer, M. Waitz, Y. Yang, G. Schiwietz, S. Zeller, T. Jahnke, and R. Dörner, J. Phys. B **50**, 034002 (2017).
[20] F. H. M. Faisal, Nat. Phys. **5**, 319 (2009).
[21] C. Liu and K. Z. Hatsagortsyan, Phys. Rev. Lett. **105**, 113003 (2010).
[22] T.-M. Yan, S. V. Popruzhenko, M. J. J. Vrakking, and D. Bauer, Phys. Rev. Lett. **105**, 253002 (2010).
[23] J. Guo, X.-S. Liu, and Shih-I. Chu, Phys. Rev. A **82**, 023402 (2010).
[24] C. Liu and K. Z. Hatsagortsyan, J. Phys. B **44**, 095402 (2011).
[25] A. Kästner, U. Saalmann, and J. M. Rost, Phys. Rev. Lett. **108**, 033201 (2012).
[26] C. Lemell, K. I. Dimitriou, X.-M. Tong, S. Nagele, D. V. Kartashov, J. Burgdörfer, and S. Gräfe, Phys. Rev. A **85**, 011403 (2012).
[27] L. Guo, S. S. Han, X. Liu, Y. Cheng, Z. Z. Xu, J. Fan, J. Chen, S. G. Chen, W. Becker, C. I. Blaga, A. D. DiChiara, E. Sistrunk, P. Agostini, and L. F. DiMauro, Phys. Rev. Lett. **110**, 013001 (2013).
[28] S. A. Kelvich, W. Becker, and S. P. Goreslavski, Phys. Rev. A **93**, 033411 (2016).
[29] D. B. Milošević, Phys. Rev. A **88**, 023417 (2013).
[30] D. B. Milošević, Phys. Rev. A **90**, 063423 (2014).
[31] W. Becker, S. P. Goreslavski, D. B. Milošević, and G. G. Paulus, J. Phys. B **47**, 204022 (2014).
[32] M. Möller, F. Meyer, A. M. Sayler, G. G. Paulus, M. F. Kling, B. E. Schmidt, W. Becker, and D. B. Milošević, Phys. Rev. A **90**, 023412 (2014).
[33] W. Becker and D. B. Milošević, J. Phys. B **48**, 151001 (2015).
[34] J. G. Leopold and I. C. Percival, J. Phys. B **12**, 709 (1979).
[35] B. Hu, J. Liu, and S. Chen, Phys. Lett. A **236**, 533 (1997).
[36] J. S. Cohen, Phys. Rev. A **64**, 043412 (2001).
[37] D. D. Hickstein, P. Ranitovic, S. Witte, X.-M. Tong, Y. Huismans, P. Arpin, X. Zhou, K. E. Keister, C. W. Hogle, B. Zhang, C. Ding, P. Johnsson, N. Toshima, M. J. J. Vrakking, M. M. Murnane, and H. C. Kapteyn, Phys. Rev. Lett. **109**, 073004 (2012).
[38] J. Liu, W. Chen, B. Zhang, J. Zhao, J. Wu, J. Yuan, and Z. Zhao, Phys. Rev. A **90**, 063420 (2014).
[39] L. V. Keldysh, Zh. Eksp. Teor. Fiz. **47**, 1945 (1964) [Sov. Phys. JETP **20**, 1307 (1965)].
[40] F. H. M. Faisal, J. Phys. B **6**, L89 (1973).
[41] H. R. Reiss, Phys. Rev. A **22**, 1786 (1980).
[42] S. V. Popruzhenko, G. G. Paulus, and D. Bauer, Phys. Rev. A **77**, 053409 (2008).
[43] S. V. Popruzhenko and D. Bauer, J. Mod. Opt. **55**, 2573 (2008).
[44] L. Torlina and O. Smirnova, Phys. Rev. A **86**, 043408 (2012).
[45] L. Torlina, M. Ivanov, Z. B. Walters, and O. Smirnova, Phys. Rev. A **86**, 043409 (2012).
[46] J. Kaushal and O. Smirnova, Phys. Rev. A **88**, 013421 (2013).
[47] M. Klaiber, E. Yakaboylu, and K. Z. Hatsagortsyan, Phys. Rev. A **87**, 023417 (2013).
[48] M. Klaiber, E. Yakaboylu, and K. Z. Hatsagortsyan, Phys. Rev. A **87**, 023418 (2013).
[49] X.-Y. Lai, C. Poli, H. Schomerus, and C. Figueira de Morisson Faria, Phys. Rev. A **92**, 043407 (2015).
[50] E. Pisanty and M. Ivanov, Phys. Rev. A **93**, 043408 (2016).
[51] T. Keil, S. V. Popruzhenko, and D. Bauer, Phys. Rev. Lett. **117**, 243003 (2016).
[52] V. S. Popov, Phys. Usp. **47**, 855 (2004).